

PACS numbers: 42.55.Ks; 42.62.Cf
DOI: 10.1070/QE2008v038n08ABEH013759

Centrifugal bubble $O_2(^1\Delta)$ gas generator with a total pressure of 100 Torr

M.V. Zagidullin, V.D. Nikolaev, M.I. Svistun, N.A. Khvatov

***Abstract*. A centrifugal bubbling singlet-oxygen gas generator is developed in which chlorine with helium are injected into the rotating layer of the alkali solution of hydrogen peroxide through cylindrical nozzles directed at an angle of 30° to the bubbler surface. The concentrations of water vapour and $O_2(^1\Delta)$ and the gas temperature were determined by using the multichannel recording of the emission bands of oxygen at 634, 703, 762 and 1268 nm. For the chlorine and helium flow rates of 60 and 90 mmol s^{-1}, respectively, the specific chlorine load of 3.2 mmol cm^{-2}, a total pressure of 100 Torr in the working region of the gas generator and the oxygen partial pressure of 36 Torr, the chlorine utilisation was 90 % and the content of $O_2(^1\Delta)$ was ~60 %. For the ratio of the flow rates of chlorine and the alkali solution of hydrogen peroxide equal to 1 mol L^{-1}, the water vapour content was ~25 %. The chemical efficiency of the oxygen – iodine laser with this gas generator achieved 23 % for the specific power of 12.7 W cm per 1 cm^3 s^{-1} per pass of the solution through the gas generator.**

Keywords: *singlet oxygen, oxygen – iodine laser, oxygen emission spectrum.*

1. Introduction

Singlet oxygen $O_2(^1\Delta)$ is a source of energy in a chemical oxygen – iodine laser. The inverse population at the $^2P_{1/2} \rightarrow {}^2P_{3/2}$ transition of the iodine atom is produced during the exchange reaction

$$O_2(^1\Delta) + I(^2P_{3/2}) \rightarrow O_2(^3\Sigma) + I(^2P_{1/2}).$$

Singlet oxygen $O_2(^1\Delta)$ is produced most efficiently in a singlet oxygen generator (SOG) in the reaction of gaseous chlorine with the alkali solution of hydrogen peroxide (hereafter, simply solution):

$$Cl_2 + 2HO_2^- \rightarrow 2Cl^- + H_2O + O_2(^1\Delta). \quad (1)$$

After passing to the gas flow from the solution, $O_2(^1\Delta)$ disappears mainly in reactions

$$O_2(^1\Delta) + O_2(^1\Delta) \rightarrow O_2(^1\Sigma) + O_2(^3\Sigma), \quad (2)$$

$$O_2(^1\Delta) + O_2(^1\Delta) \rightarrow O_2(^3\Sigma) + O_2(^3\Sigma), \quad (3)$$

$$O_2(^1\Delta) + Cl_2 \rightarrow O_2(^3\Sigma) + Cl_2, \quad (4)$$

$$O_2(^1\Sigma) + H_2O \rightarrow O_2(^1\Delta) + H_2O. \quad (5)$$

To obtain $O_2(^1\Delta)$ in reaction (1), gas – liquid mass-exchange generators of the bubbling [1], jet [2], and drop [3] types are used. For oxygen – iodine lasers of some types, of special interest are SOGs in which the components of the solution are quite efficiently spent per pass of the solution through the SOG. In this case, requirements on the recirculation system of the solution can be considerably alleviated or it can be completely excluded at all from the laser system. For a number of reasons, the above-mentioned SOGs cannot provide the efficient consumption of the components of the solution per pass though the SOG and provide simultaneously the required composition of a gas flow for the oxygen – iodine laser. After a single passage of the solution through the SOG, the absorption of 1 mmol of chlorine in 1 cm^3 of solution is accompanied by the disappearance of 30 % of singlet oxygen $O_2(^1\Delta)$ and leads to the heat release (34 kal) and the increase in temperature by 35 °C. For solution at the initial temperature $-10 \div -20$ °C heated in this way, the pressure of water vapour at the SOG output can amount to a few Torr. Therefore, the necessity of maintaining the relatively low fraction of water vapour in the active medium of a supersonic oxygen – iodine laser in the case of a large ratio of the flow rates of chlorine and solution requires the development of SOGs with a high partial oxygen pressure.

A high single-pass consumption of the solution components and the required composition of the gas flow can be provided by a centrifugal bubble SOG (CBSOG). The rotation of a gas – liquid layer in it can be produced either by the mechanical rotation of a cylindrical bubbler [4] or by introducing the gas tangentially through a set of nozzles in the immobile wall of a cylindrical reactor [5]. A two-phase gas – liquid layer in the field of centrifugal forces is characterised by the high relative velocity of the phases, the high specific surface of their contact and the efficient separation of gas from liquid. As a result, a high velocity of the interphase mass transfer is achieved and a dispersed liquid phase is efficiently removed from the gas flow. These circumstances are especially favourable for a high-pressure SOG. Note also that, unlike widely used jet and drop SOGs, the specific surface and the renovation rate of the phase contact in a CBSOG are independent of the solution flow rate. The results of the first tests of a CBSOG with the output pressure up to 20 Torr are presented in [6]. This generator was used as the energy source for an oxygen – iodine laser for the first time in papers [7, 8].

M.V. Zagidullin, V.D. Nikolaev, M.I. Svistun, N.A. Khvatov Samara Branch of the P.N. Lebedev Physics Institute, Russian Academy of Sciences, ul. Novo-Sadovaya 221, 443011 Samara, Russia;
e-mail: marsel@fian.smr.ru, nikolaev@fian.smr.ru, msvistun@fian.smr.ru

Received 12 November 2007
Kvantovaya Elektronika **38** (8) 794 – 800 (2008)
Translated by M.N. Sapozhnikov

The aim of this paper is to develop and study a CBSOG with a total output pressure of $\sim$100 Torr, the ratio of the molar flow rate of chlorine to the volume flow rate of solution up to 1 mol L^{-1}, and the specific production of oxygen equal to a few mmol s^{-1} from 1 cm^2 of the bubbler surface.

2. Experiment

The scheme of the CBSOG is presented in Fig. 1 (rotating parts of the generator are indicated in black). The CBSOG bubbler was a truncated cone (with a small angle) of diameter 60 mm and height 45 mm. Thus, unlike the CBSOG described in [6], inner volume of the bubbler was reduced by several times. Bubbler (*2*) was rotated by an electric motor with the rotation speed variable by means of a current frequency transformer. Nozzles for gas injection into the bubbler were arranged by the square-cluster method over the entire circle on a band of width 10 mm so that the working surface of the bubbler was 18.8 cm^2.

Unlike CBSOGs used in papers [6–8], the axis of cylindrical nozzles for injection of the chlorine–helium mixture into solution was directed at angle of $\alpha = 30^\circ$ to the bubbler surface. The injection of the gas at an angle to the bubbler surface reduces the initial normal component of the momentum of gas jets and causes the additional rotation of the bubble layer. The solution was prepared from the 14 M of aqueous solution of KOH and 13 M of hydrogen peroxide, so that the alkali concentration was 4.3 mol L^{-1} and the hydrogen peroxide concentration was 9 mol L^{-1}. The initial temperature T^0_{sol} of the solution before injection into the reactor was 260 K in all tests. The solution was supplied on the internal surface of the bubbler through tube (*3*) and drained out through a system of holes (*4*) and outlet (*5*) into a receiving tank. The temperature of the solution flowing from the CBSOG was measured in outlet (*5*). Perforated cylinder (*6*) of diameter 35 mm with 12 slits of a total area of 9 cm^2 was rotated on the same axis with the bubbler. The observed height h of a 'light' layer of the solution near drain holes (*4*), where gas has already separated from liquid, was determined after processing of photo and video images of the liquid layer near drain holes, which were taken through the transparent upper cover. The value of h in experiments was varied by changing the bubbler rotation frequency, the solution flow rate, and cross sections of drain holes. The gas leaving the bubbler layer flowed into chamber (*7*) through slit aperture (*8*) whose cross section could be also changed. The total volume of the gas-flow path from the bubbler surface to the slit aperture, by neglecting the height of the solution layer, was 170 cm^3, from which a free volume in the cavity of the rotating bubbler was 110 cm^3. Chamber (*7*) was a short part of the gas-flow channel of width 50 mm and height 15 mm with a slit aperture mounted at its output. By varying the cross sections of this aperture and aperture (*8*), pressures inside the CBSOG and chamber (*7*) could be changed. The gas temperature T_{gas} in the chamber was measured with a thermocouple covered by a thin layer of a silicon lubricant to reduce the deactivation of $O_2(^1\Delta)$ on its surface. The concentration N_{Cl_2} of the residual chlorine in chamber (*7*) was estimated from the attenuation of the probe radiation of a 337-nm N_2 laser.

The concentrations of water vapour and $O_2(^1\Delta)$ were determined and the gas temperature was additionally controlled by using the multichannel recording of the emission spectrum of the gas flow. An AvaSpec-3648 multichannel spectrometer (Avantes, Holland) with a fibre pigtail was used to record spectra in the range from 600 to 800 nm with a resolution of $\sim$1 nm. Emission spectra in the IR and visible ranges were recorded with a M266 spectrometer (Solar Joint-Stock Company, Belarus) with a fibre pigtail. The M266 spectrometer had two ports for coupling out radiation to an U2C-16H591 multichannel spectrum analyser (MSA) (Solar Joint-Stock Company) in the visible range with an S5931-1024S CCD linear array (Hamamatsu) and to an IR U2C-16H912 MSA (Solar Joint-

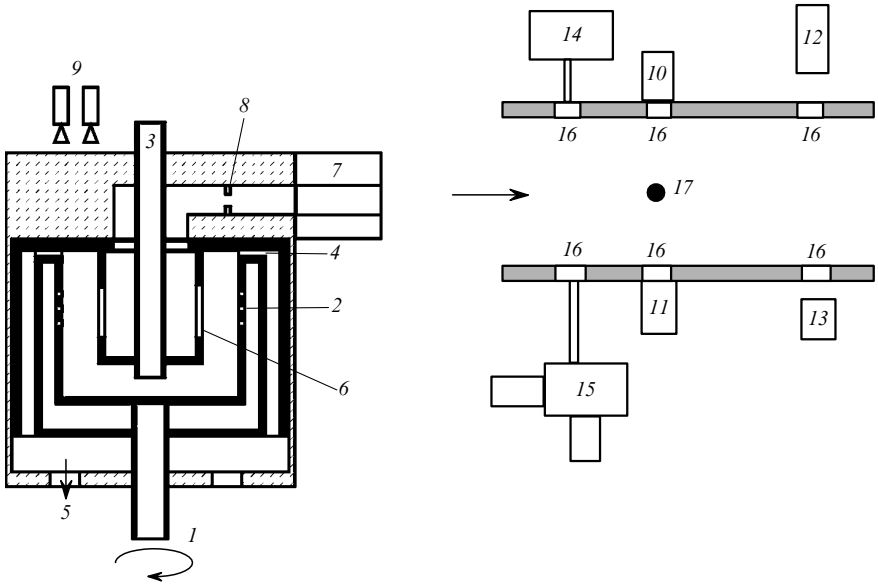

Figure 1. Scheme of the centrifugal bubble SOG: (*1*) chlorine and helium inlet; (*2*) rotating bubbler; (*3*) solution inlet; (*4*) drain holes; (*5*) drain outlet; (*6*) perforated cylinder; (*7*) measurement chamber; (*8*) slit aperture; (*9*) video and photo cameras; (*10*, *11*) germanium and silicon photodetectors; (*12*) nitrogen laser; (*13*) detector of nitrogen laser radiation; (*14*) AvaSpec-3648 spectrometer; (*15*) M266 spectrometer; (*16*) optical windows; (*17*) thermocouple.

Stock Company) with a G9212-512S InGaAs photodiode linear array (Hamamatsu).

In the visible spectral range, the dimol emission of oxygen was recorded in the 634-nm and 703-nm bands:

$$O_2(^1\Delta, v=0) + O_2(^1\Delta, v=0) \rightarrow O_2(^3\Sigma, v=0) + O_2(^3\Sigma, v=0) + hv \ (\lambda = 634 \text{ nm}), \quad (6)$$

$$O_2(^1\Delta, v=0) + O_2(^1\Delta, v=0) \rightarrow O_2(^3\Sigma, v=0) + O_2(^3\Sigma, v=1) + hv \ (\lambda = 703 \text{ nm}), \quad (7)$$

and the spontaneous emission of $O_2(^1\Sigma)$ in the 762-nm band:

$$O_2(^1\Sigma, v=0) \rightarrow O_2(^3\Sigma, v=0) + hv \ (\lambda = 762 \text{ nm}). \quad (8)$$

In the IR region, the spontaneous emission of $O_2(^1\Delta)$ at 1268 nm was recorded:

$$O_2(^1\Delta, v=0) \rightarrow O_2(^3\Sigma, v=0) + hv \ (\lambda = 1268 \text{ nm}). \quad (9)$$

Because the M266 spectrometer can operate by coupling out radiation only to one of the two ports, the 634-nm and 1268-nm emission bands were recorded by using alternately the U2C-16H591 and U2C-16H912 cameras at the same slit widths, exposure times, and CBSOG operation regimes. The spontaneous emission signals $I_1 = K_1 N_\Delta$ and $I_2 = K_2 N_\Sigma$ of $O_2(^1\Delta)$ molecules in the 1278-nm band and $O_2(^1\Sigma)$ molecules in the 762-nm band were simultaneously recorded with germanium and silicon photodetectors equipped with optical filters. Here, N_Δ and N_Σ are the concentrations of $O_2(^1\Delta)$ and $O_2(^1\Sigma)$, respectively, and K_1 and K_2 are calibration coefficients. The number of counts F recorded by the MSA at each wavelength is proportional to the number of emitted photons and is $F_{634}(\lambda) = C(\lambda)Vq_{634}(\lambda)k_6N_\Delta^2$, $F_{703}(\lambda) = C(\lambda)Vq_{703}(\lambda)k_7N_\Delta^2$, and $F_{1268}(\lambda) = C(\lambda)Vq_{1268}(\lambda)A_9N_\Delta$ for the 634-nm, 703-nm, and 1268-nm bands, respectively. Here, $C(\lambda)$ is the spectral photon sensitivity of the spectrometer; q_i are the normalised form factors of the bands taking into account the finite width the instrumental function of the spectrometer; V is the volume factor; k_6 and k_7 are the rate constants of processes (6) and (7); and A_9 the Einstein coefficient for process (9).

Because $O_2(^1\Sigma)$ is mainly quenched by water vapour, the number $F_{762}(\lambda)$ of counts detected by the MSA in the 762-nm band is proportional to the square of N_Δ and is inversely proportional to the concentration N_w of water vapour in the measurement chamber: $F_{762}(\lambda) = C(\lambda)q_{762}(\lambda)VA_8k_2N_\Delta^2/(k_5N_w)$, where k_2 and k_5 are the rate constants of processes (2) and (5), A_8 is the Einstein coefficient of process (8). The spectral photon sensitivities $C(\lambda)$ for each of the spectrometers were determined by using a SIRSh-6-40 tungsten lamp as the etalon spectral source. For the M266 spectrometer, this procedure does not introduce considerable difficulties in passing from the U2C-16H591 MSA to U2C-16H912 MSA. Calibration was performed for the same parameters of spectrometers as in the case of recording emission spectra of a gas flow from the CBSOG. For the same fibre coupling of radiation, the volume factor of a radiation source is cancelled during calibration. The concentrations of water vapour

$$N_w = \frac{f_{634}}{f_{762}}\left(\frac{A_8k_2}{k_5k_6}\right) \text{ or } N_w = \frac{f_{703}}{f_{762}}\left(\frac{A_8k_2}{k_5k_7}\right) \quad (10)$$

and molecules

$$N_\Delta = \frac{f_{634}}{f_{1268}}\frac{A_9}{k_6} \text{ or } N_\Delta = \frac{f_{703}}{f_{1268}}\frac{A_9}{k_7} \quad (11)$$

were calculated from the recorded spectra, where

$$f_i = \int \frac{F_i(\lambda)}{C(\lambda)} d\lambda$$

is the integral over the ith band, which is proportional to the total number of photons emitted in the given band. The concentration of water vapour can be also determined from the relation

$$N_w = K_3 I_1^2 / I_2, \quad (12)$$

where K_3 is the calibration coefficient. This method was used, for example, in [9].

The values of N_Δ and N_w calculated from (10) and (11) depend on the rate constants of processes and spontaneous emission probabilities A_8 and A_9. The oscillator strengths S of the 634-nm [10, 11], 762-nm [12], and 1268-nm [12, 13] bands measured by the method of absorption spectroscopy are presented in Table 1. The rate constants k_6 and Einstein coefficients A_8 and A_9 were calculated by the known expression $8\pi S(g_1/g_2)c/\lambda^2$, where S is the oscillator strength of the corresponding transition; c is the speed of light; λ is the band wavelength; g_1 and g_2 are the degeneracy multiplicities of the ground and excited states. In calculations by expressions (10) and (11), we used the average values of the Einstein coefficients A_9 (2.21×10^{-4} s^{-1}) and rate constants k_6 (6.13×10^{-23} cm^3 s^{-1}) presented in Table 1. The ratio g_1/g_2 in the calculations of k_6 for $O_2(^3\Sigma)O_2(^3\Sigma)$ and $O_2(^1\Delta)O_2(^1\Delta)$ dimers, between which the allowed dipole transition occurs in process (6), was set equal to unity, according to [14]. Because the gas temperature at the CBSOG output in rated regimes was within 290–340 K, the temperature dependence of the rate constant k_6 was neglected and its value at 295 K was used. The rate constant of reaction (5) was set equal to $(6.71 \pm 0.53) \times 10^{-12}$ cm^3 s^{-1} [15] and that of reaction (2) – to $(2.7 \pm 0.4) \times 10^{-17}$ cm^3 s^{-1} [16]. The rotational structure of the spectrum of the 762-nm band was also used to estimate the gas temperature by comparing it with the spectrum synthesised by employing the HITRAN data base [17].

Knowing N_w, N_Δ, N_{Cl_2}, the helium and chlorine flow rates, pressure P and temperature T_{gas} in the measurement chamber, we can determine the partial pressures of helium, water vapour (P_w), oxygen (P_{O_2}), residual chlorine (P_{Cl_2}), and singlet oxygen (P_Δ). These data were used to calculate the efficiency of chlorine utilisation $U = 1 - P_{Cl_2}/(P_{Cl_2} + P_{O_2})$, the relative content of water vapour $C_w = P_w/(P_{Cl_2} + P_{O_2})$, the water vapour pressure $P_{1w} = P_1P_w/P$ inside the CBSOG, and the relative content of singlet oxygen $Y = P_\Delta/P_{O_2}$ (P_1 is pressure inside the CBSOG).

3. Results

The CBSOG was tested mainly in the rated regime with the helium flow rate $M_{He} = 90$ mmol s^{-1} and chlorine flow rate $M_{Cl_2} = 60$ mmol s^{-1}. The CBSOG operated in the following way. Helium was injected into the CBSOG with the rotating bubbler, and after 2 s the solution and chlorine

Table 1.

Process	Band oscillator strength	g_1/g_2	Rate constant
(6)	$(3.19 \pm 0.03) \times 10^{-43}$ cm^4 ($T = 294$ K) [10]	1/1	$k_6 = (6.06 \pm 0.06) \times 10^{-23}$ cm^3 s^{-1}
	$(3.26 \pm 0.14) \times 10^{-43}$ cm^4 ($T = 298$ K) [11]		$k_6 = (6.2 \pm 0.3) \times 10^{-23}$ cm^3 s^{-1}
(8)	$(1.92 \pm 2) \times 10^{-22}$ cm [12]	3/1	$A_8 = (7.48 \pm 0.09) \times 10^{-2}$ s^{-1}
(9)	$(32.5 \pm 0.8) \times 10^{-25}$ cm [12]	3/2	$A_9 = (2.24 \pm 0.06) \times 10^{-4}$ s^{-1}
	$(31 \pm 1) \times 10^{-25}$ cm [13]		$A_9 = (2.18 \pm 0.07) \times 10^{-4}$ s^{-1}

were injected simultaneously. The height h of the solution layer increased continuously and achieved a stationary value after 4 s. By this moment the readings of pressure gauges, photodetectors, and a thermocouple were stabilised and the total pressure $P_1 = 100$ Torr was established inside the CBSOG. Let us presents some values of the operating parameters of a bubble layer in the region where the gas separated from the solution [i.e. near drain holes (*4*)] for the stationary value $h = 6$ mm, the solution flow rate $Q_{sol} = 105$ cm^3 s^{-1} and the rotation frequency 60 s^{-1}: the centrifugal acceleration on the bubbler surface was $G = 4.26 \times 10^4$ cm s^{-2} ($435g$, $g = 980$ cm s^{-1}), the azimuthal rotation rate was 1.13×10^3 cm s^{-1}, the total pressure on the bubbler surface was 307 Torr, the pressure gradient in the liquid was 383 Torr cm^{-1}, and the average axial rate of the solution was 10 cm s^{-1}. The velocity of the gas injected to the solution is close to the sound speed (3.2×10^4 cm s^{-1}) because the pressure of the chlorine–helium mixture in front of bubbler nozzles under these conditions was 580 Torr. The specific load on the working surface of the bubbler was 3.2 mmol cm^{-2} by chlorine and 0.24 g cm^{-2} s by mass, and the average reduced velocity of gas at the output from the bubble layer achieved 14 m s^{-1}. The flowing out of gas jets at an angle to the bubbler surface should lead to an increase in the azimuthal velocity of solution flowing on the working surface of the bubbler [18]. By neglecting the friction of the gas–liquid layer on the bubbler surface and assuming that the tangential component of the gas jet momentum is completely transferred to the solution, we obtain the increase in the azimuthal velocity of the solution

$$\frac{u_{gas}(M_{Cl} + M_{He})\mu_{gas} \cos\alpha}{Q_{sol}\rho_{liq}} \approx 940 \text{ cm s}^{-1},$$

where $u_{gas} \approx 3.2 \times 10^4$ cm s^{-1} is the velocity of the gas flow from nozzles; $\mu_{gas} = 30.8$ g mol^{-1} is the gas molar weight; $Q_{sol} = 105$ cm^3 s^{-1} is the flow rate of solution of density $\rho_{liq} = 1.3$ g cm^{-3}. This additional azimuthal velocity corresponds to the increase in the rotation velocity of the layer by 50 s^{-1}, which is comparable with the rotation frequency of the bubbler itself. It seems that this estimate can be somewhat overstated because it is necessary to take into account the friction of a gas–liquid layer on the bubbler surface [19]. Observations of the structure of the bubble layer showed that the height h^* of a gas–foam layer over gas nozzles was approximately 3–5 mm larger than the height h of a 'light' layer near drain holes. For $h \approx 8$ mm ($h^* \approx 12$ mm), the bubble layer almost achieved central perforated cylinder (*6*).

Figure 2 shows the dependence of the chlorine utilisation efficiency on the solution layer height h measured for stationary readings of all sensors. The results are presented for the solution flow rates from 50 to 200 cm^3 s^{-1}, rotation frequencies 45–80 s^{-1}, and three different cross sections of drain holes. The specific values of h were obtained for different combinations of these parameters. We found that the chlorine utilisation was mainly determined by the height h. The independence of the chlorine utilisation U on the centrifugal acceleration G can be qualitatively explained by the increase in the working surface of the contact of phases along with the shortening of the contact time between gas and liquid with increasing G [4]. The additional rotation of the bubble layer caused by the tangential momentum of the gas also can remove the dependence of the chlorine utilisation on the rotation frequency of the bubbler. The dependence of the chlorine utilisation on h can be approximately described by the expression $U = 1 - \exp(-0.41h)$, where h is measured in mm. For $h \approx 2$ mm, when the velocity of an insufficiently expanded gas jet flowing into the solution is equal to the sound speed, more than 50 % of chlorine is absorbed in a gas–foam layer. The acid–alkali titration of the spent solution showed that the amount of utilised chlorine completely coincided with the change in the amount of HO_2^- ions in the solution flowing from the CBSOG according to the stoichiometry of reaction (1).

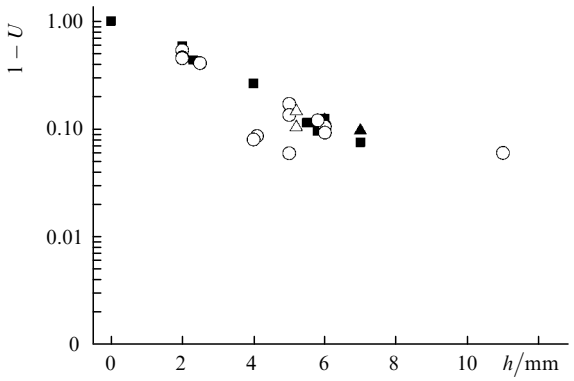

Figure 2. Dependence of the chlorine utilisation on the height h of the solution layer for $M_{Cl_2} = 60$ mmol s^{-1}, $M_{He} = 90$ mmol s^{-1}, and the bubbler rotation frequencies 45–49 (▲), 60–64 (■), 67–73 (○), and 75–80 s^{-1} (△).

Figure 3 presents the emission spectra of oxygen recorded with a M266 spectrometer. The spectra were recorded during two successive runs with the chlorine flow rate of 50 mmol s^{-1} and completely identical working parameters of the CBSOG. The exposure time used in both MSAs was 4 s. The identical flow parameters in chamber (*7*) were provided by controlling the gas flow rate, pressure P, the residual chlorine, and the output spontaneous emission signals I_1 and I_2 of $O_2(^1\Delta)$ and $O_2(^1\Sigma)$. These parameters in the two runs differ by no more than 5 %. The ratio f_{634}/f_{1268} for the spectra presented in Fig. 3 is 0.0747, which gives $N_\Delta = 2.7 \times 10^{17}$ cm^{-3}. The calculation of N_Δ by using the spectra obtained during several identical runs of the CBSOG gave the scatter of the values of N_Δ within $\pm 1.44 \times 10^{16}$ cm^{-3}, or the relative error 5 %. The gas

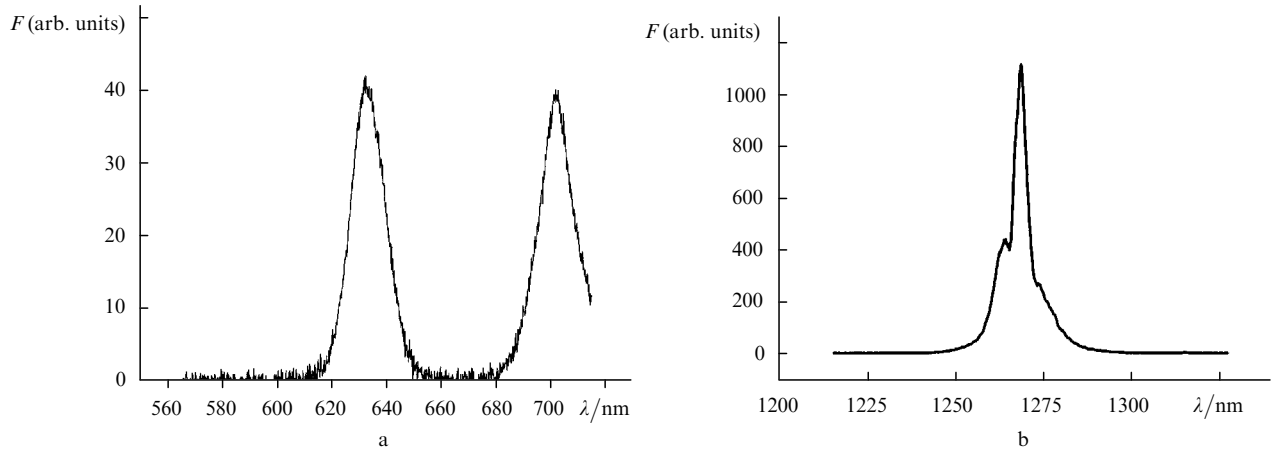

Figure 3. Emission bands of oxygen at 634, 703 nm (a) and 1268 nm (b).

temperature measured with a thermocouple in these regimes was $T_{gas} = 310$ K and the partial pressure of oxygen in the chamber was $P_{O_2} = 15$ Torr, which gives $Y = 57\,\%$. The output signal I_1 of a germanium photodetector was 0.46 ± 0.01 V. Because $I_1 = K_1 N_\Delta$, we obtain the reciprocal value of the calibration coefficient $K_1^{-1} = 5.87 \times 10^{17}$ cm^{-3} V^{-1} with an accuracy of 7 % for measuring the concentration of $O_2(^1\Delta)$ by the output signal of I_1 the germanium photodetector. The calculation error of N_Δ determined by the uncertainty in the values of k_6 and A_9 is $\sim 8\,\%$. Thus, the total relative measurement error of N_Δ is $\sim 13\,\%$ and of $K_1 \sim 15\,\%$.

Figure 4 presents the dependence of the singlet oxygen yield Y on the height h of the 'light' bubble layer. The value of Y in chamber (*7*) depends on several factors: the deactivation of $O_2(^1\Delta)$ in the liquid phase, quenching in processes (2)–(5) during the propagation of the gas through the bubble layer and its transport to chamber (*7*). After the separation of the gas from the bubble layer, the content of $O_2(^1\Delta)$ in it decreases due to reactions (2)–(4). The increase in the height h is accompanied by a decrease in the free volume inside the bubbler and in the time of gas transport to the slit aperture, which reduces the loss of $O_2(^1\Delta)$. For example, for $h = 6$ mm, the free volume in the rotating part of the bubbler decreases from 110 to 64 cm^3 and the gas flight time from the bubbler surface to slit (*8*) is 4.5×10^{-3} s. As h increases from 4 to 10 mm, the characteristic quenching parameter of $O_2(^1\Delta)$ in reactions (2) and (3) at the oxygen pressure of 36 Torr changes from 0.18 to 0.13 Torr s at the transport interval to the slit aperture. Thus, a weak decrease in Y observed with increasing h is explained by the increasing loss of $O_2(^1\Delta)$ inside the bubble layer.

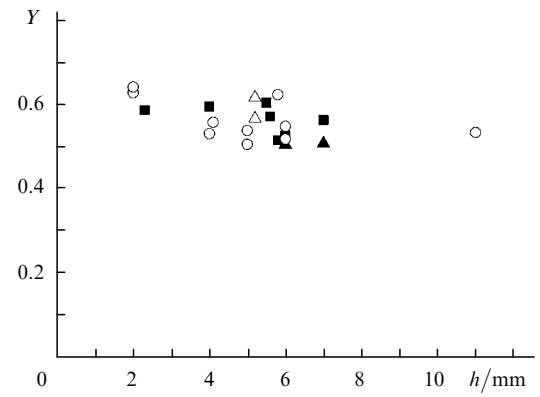

Figure 4. Dependence of the $O_2(^1\Delta)$ content on the height h for $M_{Cl_2} = 60$ mmol s^{-1}, $M_{He} = 90$ mmol s^{-1}, $P_1 = 100$ Torr, and the bubbler rotation frequencies 45–49 (▲), 60–64 (■), 67–73 (○), and 75–80 s^{-1} (△).

However, a substantial decrease in the $O_2(^1\Delta)$ yield is observed only for $h \approx 10$ mm. For fixed h, the partial pressure of oxygen inside the bubble layer increases with increasing the rotation frequency and the rates of reactions (2)–(4) increase. The absence of the distinct dependence of Y on the rotation frequency in this case can be explained by the shortening of the gas residence time in the bubble layer with increasing G. The additional 'rotation' of the bubble layer by the tangential momentum of the gas also masks this dependence.

Figure 5 presents the emission spectrum of oxygen in the region from 600 to 800 nm recorded with an AvaSpec-3648 spectrometer for determining the rotational temperature of $O_2(^1\Sigma)$ and the concentration N_w of water vapour. The flow temperature depends on the amount of quenched $O_2(^1\Delta)$, which was varied in experiments by changing the chlorine flow rate and the cross section of aperture (*8*). A comparison of the rotational structure in the 762-nm band with the synthesised spectrum gives the rotational temperature of $O_2(^1\Sigma)$ with an accuracy of ± 10 K. We found that the temperature $T_{gas} = 330 - 340$ K measured with a thermocouple in the rated operation regimes of the CBSOG ($M_{Cl_2} = 60$ mmol s^{-1}, $M_{He} = 90$ mmol s^{-1}, $P_1 = 100$ Torr) coincided with the rotational temperature of $O_2(^1\Sigma)$. At higher temperatures ($T_{gas} = 370$ K), the rotational temperature of $O_2(^1\Sigma)$ was equal to 400 K, and for $T_{gas} = 310$ K it was equal to 280 K. These differences in the temperatures suggest that the systematic error is introduced to the thermocouple readings by the thermocouple heating during $O_2(^1\Delta)$ quenching on its surface and heat removal through the supply wires of the thermocouple. The measurements of f_{703} and f_{634} for 20 runs of the CBSOG gave the ratio $f_{703}/f_{634} = 1.06 \pm 0.02$, i.e. the rate constant of process (7) $k_7 = (1.06 \pm 0.02)k_6$. A similar relation for the rate constants of processes (6) and (7) was obtained in paper [20].

The solution in the CBSOG is heated in reaction (1) during the quenching of $O_2(^1\Delta)$ in the solution and gas phase in reactions (2)–(4) and due to heat exchange between the gas and solution. During the propagation of the solution through the bubble layer, the solution temperature increases

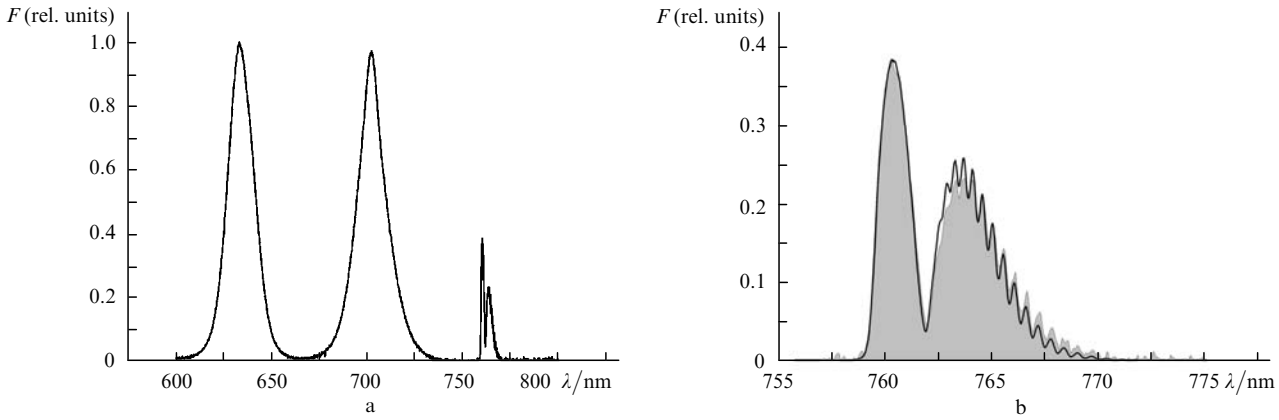

Figure 5. Emission bands of oxygen at 634, 703, and 762 nm (a) and the 762-nm band recorded at the expanded scale (the area of experimental spectrum is hatched, the curve shows the spectrum synthesised at the rotational temperature of $O_2(^1\Sigma)$ equal to 340 K) (b).

and the pressure of water vapour in the gas leaving the solution rises. After the complete separation of the gas, the solution acquires the output temperature $T_{sol\,1}$, which is the higher, the higher is the ratio UM_{Cl_2}/Q_{sol}. We measured the temperature of the solution flowing from the CBSOG by changing the ratio UM_{Cl_2}/Q_{sol} by varying the flow rates of the solution and chlorine. The concentration of water vapour in chamber (*7*) was calculated from (10) and then the pressure P_{1w} of water vapour inside the CBSOG was found. The dependence of P_{1w} on the temperature $T_{sol\,1}$ of solution flowing from the CBSOG is presented in Fig. 6. By summing all errors of the rate constants in (10), we obtain the measurement error for P_{1w} of $\sim$30 %. The pressure of water vapour inside the CBSOG calculated by the average values of rate constants in (10) exceeds somewhat the average logarithmic pressure of water vapour for the initial ($T_{sol\,0}$) and output ($T_{sol\,1}$) temperatures of the solution:

$$P_w^{ln} = \frac{P_{sat}(T_{sol\,1}) - P_{sat}(T_{sol\,0})}{\ln[P_{sat}(T_{sol\,1})/P_{sat}(T_{sol\,0})]},$$

where P_{sat} (Torr) $= 9.26 \times 10^8 \exp(-5388.5/T)$ is the pressure of the saturated vapour for the given composition of the solution at temperature T. At the temperatures of the outgoing solution near 290 K, the pressure P_{1w} is considerably lower than the saturated pressure for the output temperature $T_{sol\,1}$. The calibration coefficient K_3 for the calculation of the water vapour pressure by (12) was determined from the values of I_1, I_2, and P_w.

The content of water vapour in the rated operation regimes of the CBSOG ($M_{Cl_2} = 60$ mmol s^{-1}, $M_{He} = 90$ mmol s^{-1}, $P_1 = 100$ Torr) was determined for different flow rates Q_{sol} of the solution. Figure 7 presents the dependence of the relative content of water vapour on the amount of chlorine utilised in 1 L of the solution propagated through the CBSOG. The content of water vapour was approximately 25 % of the total of the pressures of oxygen and residual chlorine for the ratio $UM_{Cl_2}/Q_{sol} \approx 1$ mol L^{-1}. For the entire range of values of $UM_{Cl_2}/Q_{sol} = (0.2 - 1)$ mol L^{-1}, the value of Y was higher than 50 % and the chlorine utilisation was $\sim$90 % for the bubble layer height of about 6 mm. For $UM_{Cl_2}/Q_{sol} = 1$ mol L^{-1} and $U = 90$ %, the concentration of HO_2^- ions in the solution decreases by 1.8 mol L^{-1} from the initial value 4.3 mol L^{-1}, i.e. more than 40 % of HO_2^- ions were spent per pass of the solution through the reactor.

To find large-dispersion drops of the solution in the gas flow from the CBSOG, an aerosol trap representing a four-layer grid with a cell of size 10 μm overlapping the entire gas-flow channel was placed behind slit (*8*). Ten runs of a total duration of 50 s were performed with the flow rates $M_{Cl_2} = 60$ mmol s^{-1} and $M_{He} = 90$ mmol s^{-1} at the rota-

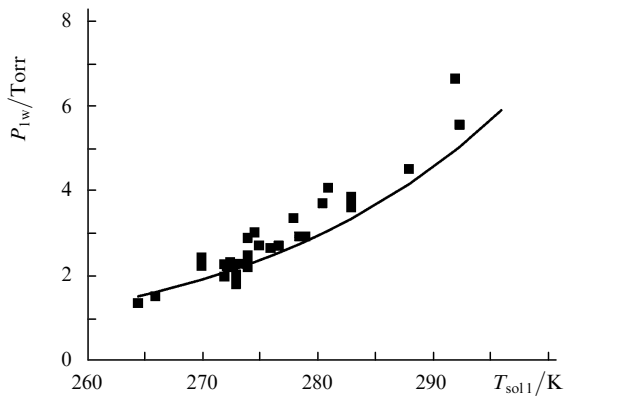

Figure 6. Water vapour pressure P_{1w} (■) inside the CBSOG as a function of the output temperature $T_{sol\,1}$ of the solution; the solid curve is the mean logarithmic pressure of water vapour pressure.

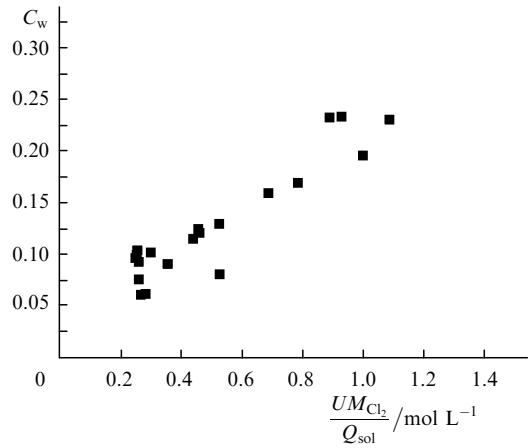

Figure 7. Relative content C_w of water vapour as a function of the parameter UM_{Cl_2}/Q_{sol} for $P_1 = 100$ Torr, $M_{Cl} = 60$ mmol s^{-1} and $M_{He} = 90$ mmol s^{-1}.

tion frequencies of the bubbler from 60 to 85 s^{-1}. No signs of deposited drops or their dry residue were observed in the trap. Then, the grid was rinsed in 100 mL of distilled water and the content of alkali in this probe was determined by the method of acid–alkali titration. It was found that less than 10^{-5} mol of KOH remained on the grid. For the total mass of the gas escaped from the CBSOG equal to 230 g, we obtain that the relative mass fraction of the dispersed solution carried away by the gas is less than 3×10^{-3} g. It is not inconceivable that a greater part of solution deposited on the grid reacted with residual chlorine and the residue was the KCl salt. The measurement of the specific resistance of the probe showed that the total amount of the salt deposited on the grid was 1.3×10^{-4} mol. At the concentration of potassium in the solution equal to 4.3 mol L^{-1}, this corresponds to the total mass of the carried away solution equal to 0.033 g or the mass fraction of 1.4×10^{-4}. By assuming that all the drops of size more than 10 μm are separated in the trap, we can conclude that the total mass fraction of such drops in the gas flow was less than 1.4×10^{-4}. However, it is known that the size of particles carried away in centrifugal bubble reactors and their mass fraction increase with increasing G. For example, it was shown in [21] that for $G = 2 \times 10^3$ m s^{-2} the average size of particles carried away by the gas flow was smaller than 1 μm and their mass fraction could be $\sim 10^{-3}$.

The CBSOG developed in our work was used in an oxygen–ion laser with the ejector nozzle bank [8]. For the chlorine flow rate of 48.8 mmol s^{-1} and the solution flow rate of 80 mmol s^{-1} in the CBSOG, the chemical efficiency of the laser achieved ~23 % for the specific power of 12.7 W per 1 cm^3 s^{-1} of the solution consumption, which is twice as large as the result achieved in [8].

4. Conclusions

The CBSOG with a high specific chlorine load per bubbler unit area and a high single-pass consumption of components in the alkali solution of hydrogen peroxide has been developed. The concentrations of water vapour and $O_2(^1\Delta)$ molecules in the gas flowing out of the CBSOG have been measured by using the multichannel recording of spectra in the regions from 600 to 800 nm and 1268 nm. A specific feature of the CBSOG is the injection of the gas at the subsonic speed into the solution layer at an angle to the rotating bubbler surface, which leads to the additional rotation of the bubble layer and a decrease in the normal momentum of injected gas jets. The mass fraction of the liquid phase (drops of size more than 10 μm) in the gas flow is $\sim 10^{-4}$ for the specific gas load up to 0.24 g cm^{-2} s and the average reduced gas velocity at the output from the bubble layer equal to 14 m s^{-1}. For the chlorine flow rate of 60 mmol s^{-1}, the change in the centrifugal acceleration within $G = 2.4 \times 10^3 - 7.5 \times 10^3$ m s^{-2} weakly affects the chlorine utilisation efficiency. As the height h of the 'light' layer increases, the chlorine utilisation efficiency increases above 90 % for $h = 6 - 8$ mm and the specific chlorine load up to 3.2 g cm^{-2} s. The $O_2(^1\Delta)$ yield in the range of centrifugal accelerations $G = 2.4 \times 10^3 - 7.5 \times 10^3$ m^3 s^{-2} is independent of G and decreases with increasing h. For the bubble layer height $h \approx 6$ mm, oxygen pressure at the CBSOG output of 36 Torr, and the chlorine utilisation efficiency of 90 %, the $O_2(^1\Delta)$ content is ~60 %. The pressure of water vapour at the CBSOG output exceeds somewhat the mean logarithmic pressure at the initial and final solution temperatures, but at high $T_{sol\,1}$ it is considerably lower than the pressure of saturated vapour at the output temperature of the solution. The water vapour pressure at the CBSOG output increases with increasing the ratio UM_{Cl_2}/Q_{sol}, and for $UM_{Cl_2}/Q_{sol} = 1$ mol L^{-1} the water vapour content is ~25 %. In this case, the single-pass consumption of solution components achieves 40 %. The chemical efficiency of the oxygen–iodine laser with this CBSOG achieved 23 % for the specific power of 12.7 W per 1 cm^3 s^{-1} per single pass in the gas generator.

Acknowledgements. The authors thank E.V. Fomin and P.A. Mikheev for processing of the emission spectra of oxygen. This work was partially supported by the European Office of Aerospace Research and Development (EORAD) (Project No. 057003), the International Scientific and Technology Center (Grant No. 3380P), and the Russian Foundation for Basic Research (Grant No. 08-08-99064).

References

1. Vagin N.P., Kryukov P.G., Yuryshev N.N. *Kvantovaya Elektron.*, **12**, 1921 (1985) [*Sov. J. Quantum Electron.*, **15**, 1268 (1985)].
2. Zagidullin M.V., Kurov A.Yu., Kupriyanov N.L., Nikolaev V.D., Svistun M.I., Erasov N.V. *Kvantovaya Elektron.*, **18**, 826 (1991) [*Sov. J. Quantum Electron.*, **21**, 747 (1991)].
3. Trayer W.J. *AIAA Paper № 92-3008* (1992).
4. Safonov A.I., Krylov V.S. *Zh. Prikl. Khim.*, **50**, 2288 (1977).
5. Burdukov A.P., Gol'dshtik M.A., Dorokhov A.R., Kazakov V.I., Li T.V. *Zh. Prikl. Mekh. Tekh. Fiz.*, **6**, 129 (1981).
6. Zagidullin M.V., Nikolaev V.D., Svistun M.I., Khvatov N.A. *Inzhener. Fiz. Zh.*, **80**, 121 (2007).
7. Zagidullin M.V., Nikolaev V.D., Svistun M.I., Hager G.D. *Appl. Phys. Lett.*, **86**, 25 (2005).
8. Zagidullin M.V., Nikolaev V.D., Svistun M.I., Khvatov N.A. *Kvantovaya Elektron.*, **35**, 907 (2005) [*Quantum Electron.*, **35**, 907 (2005)].
9. Bonnet J., Gorges E., Leporcq B., Pigache D., Verdier C. *Appl. Phys. Lett.*, **45**, 1009 (1984).
10. Naus H., Ubachs W. *Appl. Opt.*, **38**, 3423 (1999).
11. Tiedje H.F., DeMille S., MacArtur L., Brooks R.L. *Can. J. Phys.*, **79**, 773 (2001).
12. Cheah S., Lee Y., Ogilvie J.F. *J. Quantum. Spectr. Rad. Trans.*, **64**, 467 (2000).
13. Newman S.M., Lane I.C., Orr-Ewing A.J., Newnham D.A., Ballard J. *J. Chem. Phys.*, **110**, 10749 (1999).
14. Borrell P., Rich N.H. *Chem. Phys. Lett.*, **99**, 144 (1983).
15. Aviles R.G., Muller D.F., Houston P.L. *Appl. Phys. Lett.*, **37**, 358 (1980).
16. Lilenfeld H.V., Carr P.A.G., Hovis F.E. *J. Chem. Phys.*, **81**, 5730 (1984).
17. Rothman L.S., Jacquemart D., Barbe A., Benner D.C., Birk M., Brown L.R., Carleer M.R., Chackerian C., Chance K., Coudert L.H., Dana V., Devi V.M., Flaud J.-M., Gamache R.R., Goldman A., Hartmann J.-M., Jucks K.W., Maki A.G., Mandin J.-Y., Massie S.T., Orphal J., Perrin A., Rinsland C.P., Smith M.A.H., Tennyson J., Tolchenov R.N., Toth R.A., Vander Auwera J., Varanasi P., Wagner G. *J. Quantum Spec. Rad. Trans.*, **96**, 139 (2005).
18. Gol'dshtik M.A., Li T.V., Khanin V.M., Smirnov N.P. *Protsessy perenosa v energokhimicheskikh mnogofaznykh sistemakh* (Transfer Processes in Energochemical Multiphase Systems) (Novosibirsk, Institute of Thermal Physics, Siberian Branch, RAS, 1983) p. 93.
19. Shilyaeva M.I., Dorokhov A.R. *Teplofiz. Aeromekh.*, **5**, 189 (1998).
20. Whitelow S.H., Findlay F.D. *Can. J. Chem.*, **45**, 2087 (1967).
21. Nechaev N.G. *Sibir. Fiz.-Tekh. Zh.*, **1**, 86 (1991).